Electronic Supplementary Material (ESI) for Physical Chemistry Chemical Physics.

Supplementary Information

Investigation of the Water Stimulated Mg^{2+} Insertion Mechanism in an Electrodeposited MnO_2 Cathode using X-ray Photoelectron Spectroscopy

Emily Sahadeo[1], Jaehee Song[1], Karen Gaskell[1], Nam Kim[1], Gary Rubloff[2,3], and Sang Bok Lee[1]*

1. Department of Chemistry and Biochemistry, University of Maryland, College Park, Maryland, 20742, USA
2. Department of Materials Science and Engineering, University of Maryland, College Park, Maryland, 20742, USA
3. Institute for Systems Research, University of Maryland, College Park, Maryland, 20742, USA

*slee@umd.edu

Angle-Resolved XPS (AR-XPS)

Although the inelastic mean free paths (IMFP) of the electrons in the mixed material examined in this work are not known, a general description of how take-off angle (TOA) affects the surface sensitivity of AR-XPS can be provided. For instance, if it is assumed that the escape depth (ED) for our samples- which is equal to 3λ where λ=IMFP - is 6 nm, the depth examined at different angles can be calculated according to $d=EDsin\theta$. In this equation, d is the depth of the sample probed and θ is the TOA with respect to the sample surface. For instance, using this equation the depth examined at 50° would be 4.60 nm, while at 20° it would be 2.05 nm. Therefore, we can mathematically see how the depth examined is decreasing with a decreasing TOA relative to the sample surface in a general case.

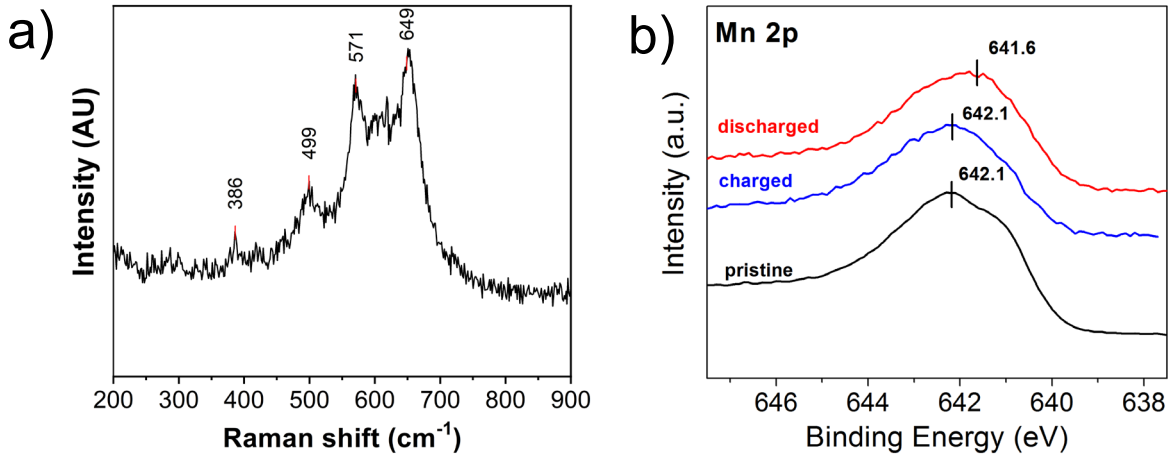

Figure S1. a) Raman spectrum of as-deposited MnO_2 on the Pt-sputtered AAO b) Mn 2p XPS spectra for pristine MnO_2, and electrodes charged and discharged after 10 CV cycles in 0.1 M $Mg(ClO_4)_2 \cdot 6H_2O$/PC electrolyte.

Figure S1a shows that despite a lack of long-range order, the Raman modes observed for the film indicate that there may be small domains that contain birnessite structured MnO_2.[1] The noise in the spectrum can be attributed to the small amount of material in the thin film morphology, as well as the necessity of using a low laser power to prevent annealing of the sample with the laser. To provide some evidence of Mn oxidation and reduction, the Mn $2p_{3/2}$ XPS spectra are illustrated in Figure S1b. The peak broadening upon discharge are due to larger contribution from low-binding energy signals which indicate a reduction of the Mn to a lower oxidation state upon discharge.[2] This oxidation state change is reversible, as seen from the shift back to a higher binding energy upon charging of the electrode.

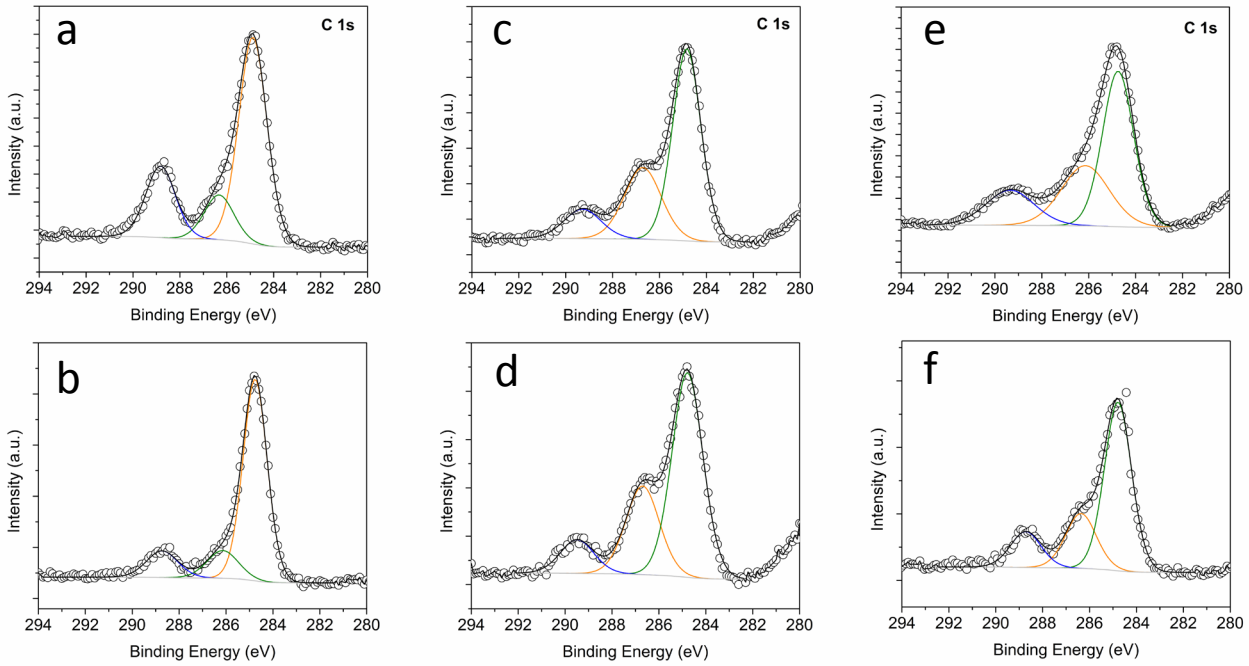

Figure S2. C 1s spectra for samples illustrated in Figure 2 of the main text. (a) Pristine MnO_2, (b) MnO_2 discharged in dry electrolyte (c) MnO_2 discharged using CV (d) MnO_2 in charged state after CV (e) discharged using CA (f) charged using CA. The three main components consist of C-C and C-H at 284.8 eV, C-O species at ~286.5 eV, and carboxyl species at 289 eV.

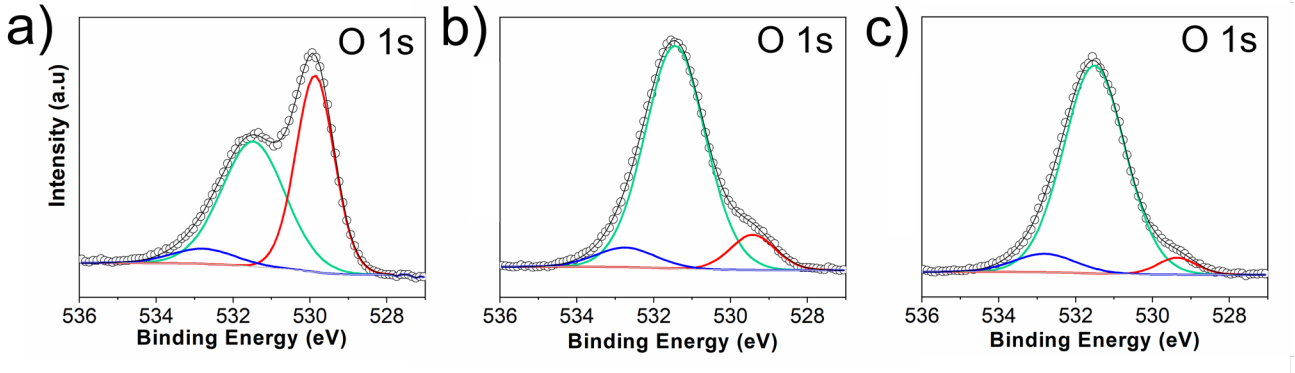

Figure S3. High-resolution and angle-resolved XPS results for electrodes in aqueous $Mg(ClO_4)_2$ electrolyte. (a) Charged MnO_2 via CA method, 90° take-off angle (b) discharged MnO_2 via CA, 90° take-off angle (c) discharged MnO_2, 20° take-off angle. The 20° sample is not shown for the charged sample as there were no significant differences between 90° and 20°.

For electrodes discharged in aqueous electrolyte, there is a notable decrease in oxide species going from 90° (Figure S3b) to 20° (Figure S3c), supporting the formation of hydroxides nearer to the surface when water is present in the electrolyte. The hydroxide formation is reversible upon charging as can be seen from the re-appearance of the oxide peak and decrease in hydroxide species in the charged sample (Figure S3a).

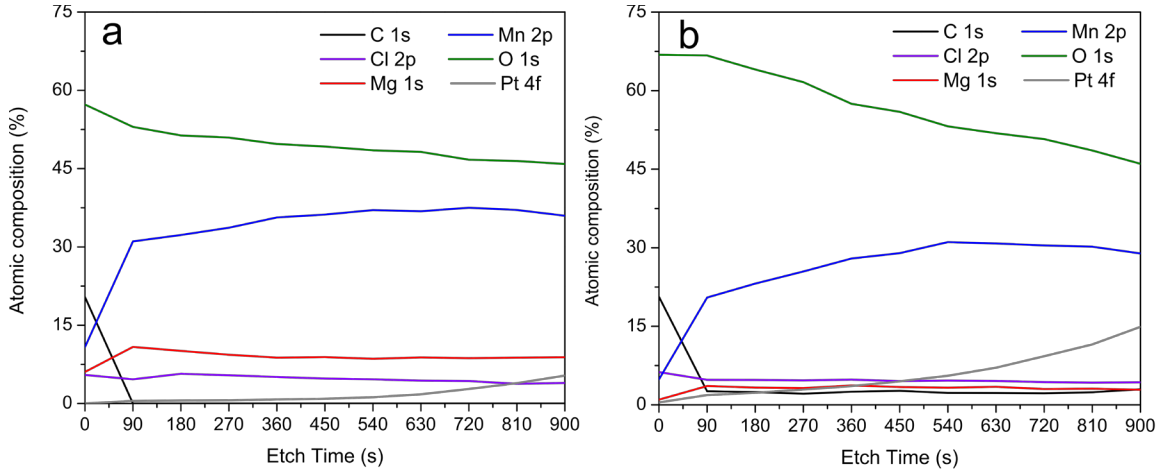

Figure S4. Depth profiles of all elements in the a) discharged and b) charged MnO_2 electrodes in 0.1 M $Mg(ClO_4)_2 \cdot 6H_2O$/PC electrolyte after 10 CV cycles.

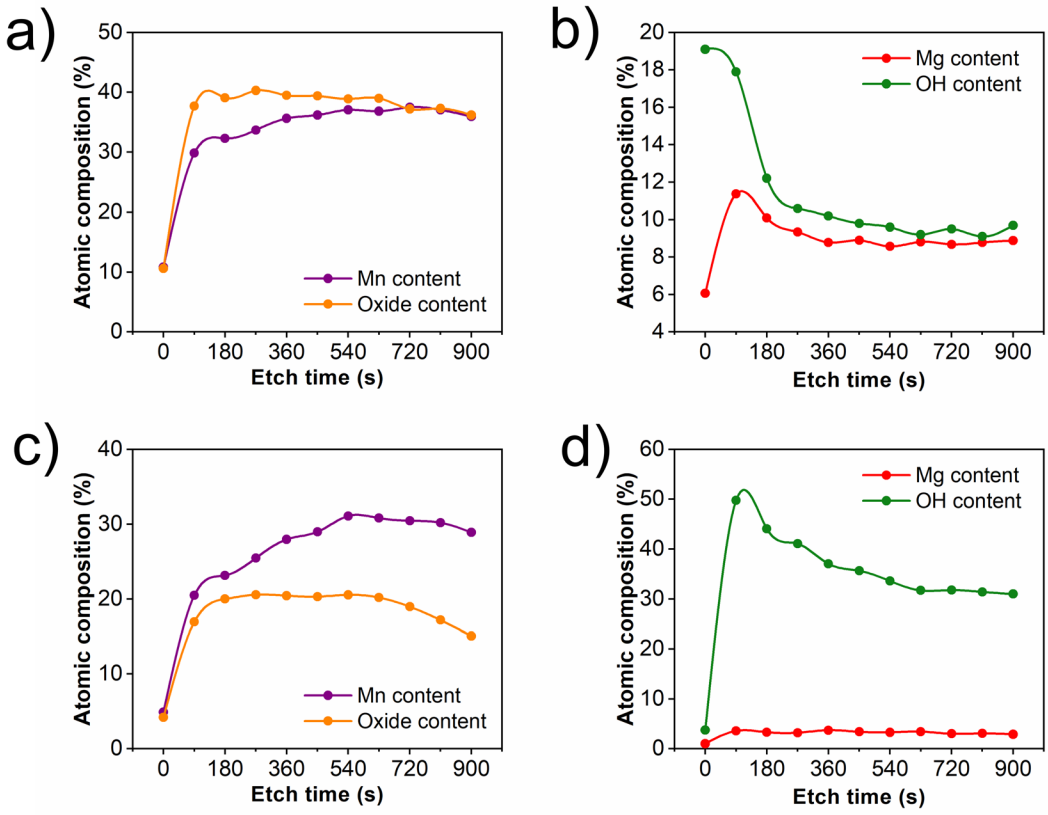

Figure S5. XPS depth profile comparisons of Mn content (Mn 2p), Mg content (Mg 1s) and oxide and hydroxide content (O 1s). Comparisons for AD-MnO_2 are depicted in (a) and (b), while comparisons for AC-MnO_2 are in (c) and (d).

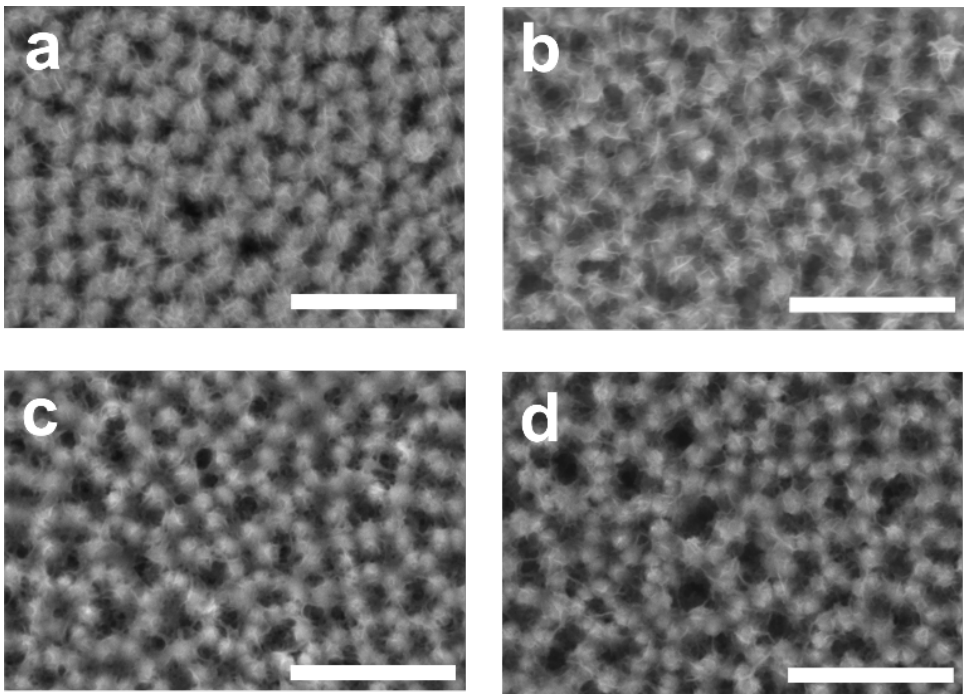

Figure S6. SEM images of electrodeposited MnO_2 in a) its pristine form, b) AD-MnO_2 cycled in dry electrolyte for 2 cycles c) AC-MnO_2 cycled in dry electrolyte for 2 cycles, both a and c after cycling. in 0.1M $Mg(ClO_4)_2{\cdot}6H_2O$ in PC for 10 cycles, and d) pristine MnO_2 cycled in dry electrolyte for 2 cycles. All scale bars are 500 nm. Some loss of MnO_2 can be seen visually in c and d, while b remains mostly unchanged, indicating the presence of water may help decrease MnO_2 destruction and dissolution.

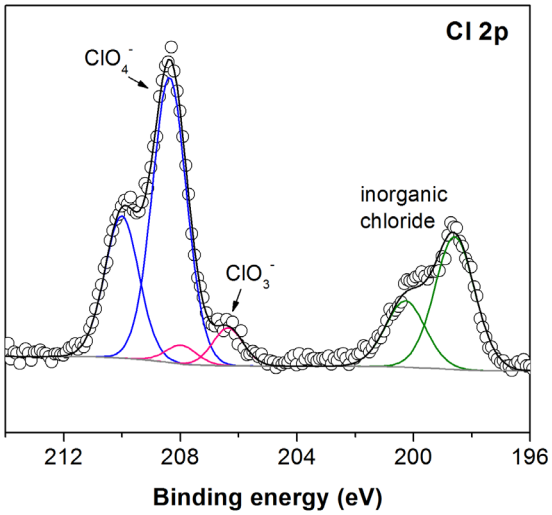

Figure S7. Cl 2p XPS spectra for MnO_2 in the discharged state after 10 CV cycles in 0.1 M $Mg(ClO_4)_2 \cdot 6H_2O$/PC, then 2 cycles in dry 0.1 M $Mg(ClO_4)_2$/PC. Perchlorate and chlorate species disappear upon depth profiling after the first 90 second etch step.

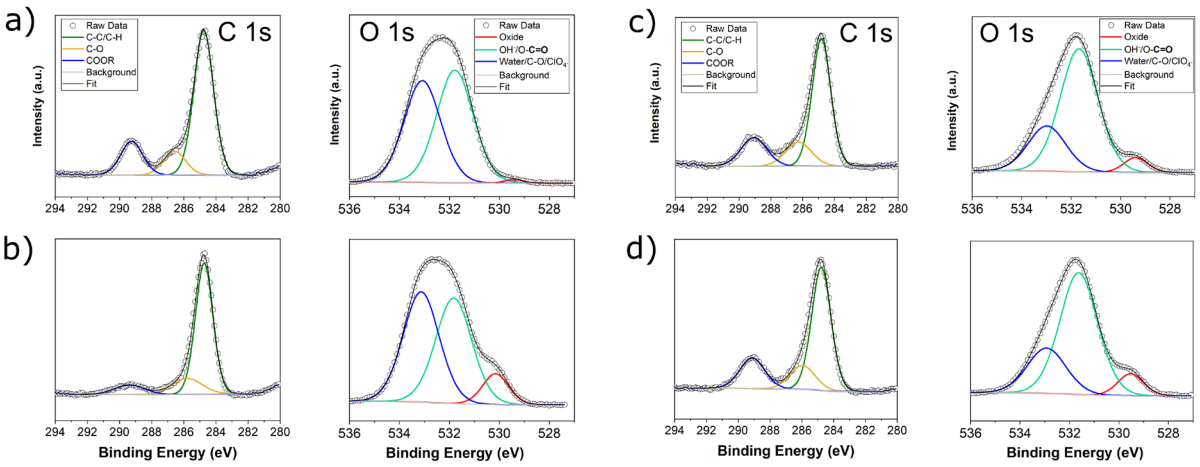

Figure S8. XPS results for O 1s and C 1s regions of two MnO_2 samples discharged using CA tested before and after air exposure. a) 15 mC MnO_2 deposited and discharged, XPS taken with no air exposure b) same sample from (a) after 24 hours of air exposure c) 5 mC MnO_2 deposited and discharged, XPS taken with no air exposure d) same sample from (c) after 24 hours of air exposure.

To test the effect of air exposure, two MnO_2 samples of different thicknesses (one deposited by passing 15 mC of charge, the other was deposited by passing 5 mC of charge) were first electrochemically treated outside of the glovebox in the same manner as described in the experimental section. However, after being rinsed with PC to remove salt species, they were transferred directly to the antechamber of a MBRAUN glovebox with <0.5 ppm water and oxygen instead of being moved into a vacuum desiccator. The electrodes were still wet with PC during transfer to prevent as much air exposure as possible. They were also transferred from the glovebox to a glove bag attached to the XPS vacuum chamber without any air exposure. With these precautions, the samples were not exposed to air. After taking the XPS spectra in Figure S8a and c, both samples were removed from the glovebox and allowed to sit in the atmosphere exposed to air and humidity for 24 hours. The XPS spectra in Figure S8c and d were then taken. This amount of exposure was done as an extreme case, as at most the samples in our paper were exposed to air for 10 minutes during transfer to the XPS.

Examining the XPS data after air exposure, it is apparent that there are not major changes to the samples. The 15 mC deposited sample saw an increase in the amount of oxide present and a decrease in the amount of Mg, which may indicate oxidation of Mn by the atmosphere. There was a small amount of this effect seen in the 5 mC sample, but very minor. However, this oxidation does not significantly alter our analysis or conclusions – air exposure cannot account for the $Mg(OH)_2$ formation according to these results. Additionally, this Mn oxidation would in fact make our expected results less pronounced if the Mg ions diffuse into the bulk of the MnO_2 and away from the surface upon air exposure. While not shown here, the binding energies of the Mg 1s regions did not shift more than 0.2 eV after air exposure, which is within the margin of error and confirms the stability of the $Mg(OH)_2$ layer upon air exposure. Detailed atomic composition results are shown in Table S1.

Table S1. Atomic composition results determined from XPS for MnO_2 samples before and after air exposure

	% Composition							
			O 1s			C 1s		
	Mg 1s	Mn 2p	H_2O/C-O/ClO_4^-	OH/C=O	O^{2-}	C-C/C-H	COOR	C-O
15 mC AD-MnO_2, CA	8.2	1.2	21.6	23.9	0.4	28.1	5.2	7.4
15 mC AD-MnO_2, CA (air)	5.9	4.6	22.2	21.3	4.5	27.0	5.7	3.4
5 mC AD-MnO_2, CA	12.1	2.8	11.5	31.2	2.4	24.0	6.3	7.5
5 mC AD-MnO_2, CA (air)	11.9	3.9	11.7	30.6	3.8	22.9	5.7	7.4

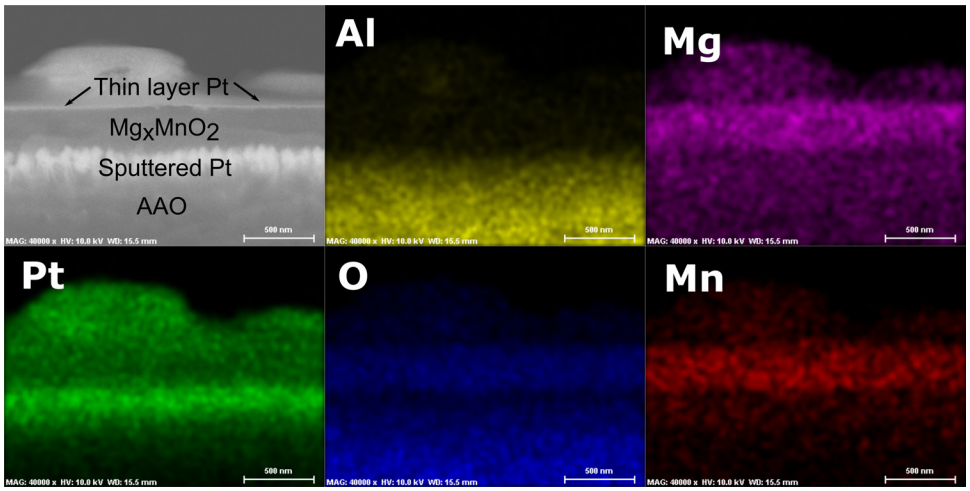

Figure S9. SEM-EDS maps for a 300 nm thick film of MnO_2 discharged using the CA method

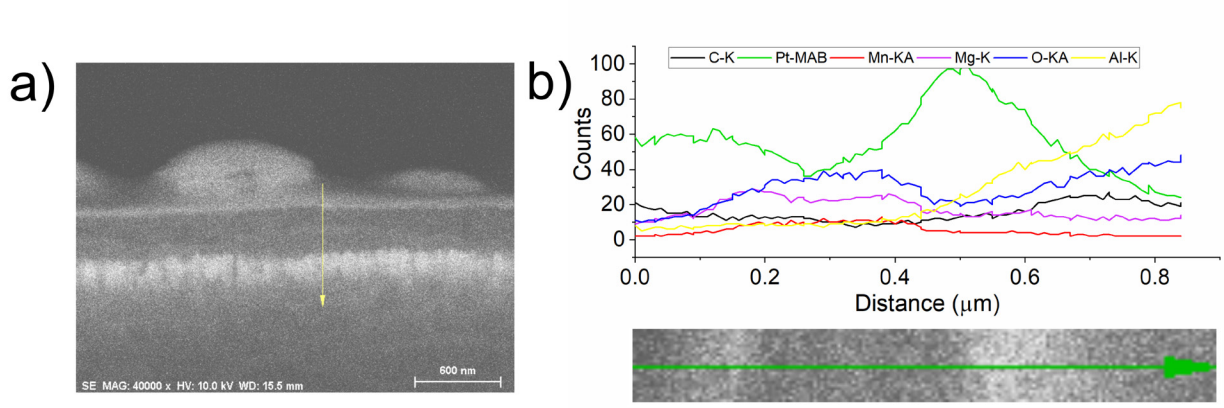

Figure S10. SEM-EDS line scan results for 300 nm thick MnO_2 film discharged using the CA method. a) SEM image where the yellow arrow indicates the region for the line scan b) line scan counts for the elements detected in the thin film with a zoomed-in image of the line scan region.

To collect the SEM images and perform the Energy Dispersive X-ray Spectrometry (EDS) analysis, thicker MnO_2 films were deposited by passing significantly more charge (50 mC) than used for thin film XPS analysis because the thin (~50 nm) films would be difficult to see using SEM. The ~300 nm thick film was discharged by holding the potential at -0.4 V vs. Ag/AgCl for 5 minutes, the same CA method used on thin films. The cross-section was exposed by cracking the AAO which supports the film in half, and mounting it so the cross-section could be seen via SEM. A thin layer of platinum was put on top of the film via a gas injection system to protect the interface of MnO_2/AAO, which was then polished using a Xe focused ion beam in a Tescan XEIA FIB/SEM instrument. The sample

was then covered in a very thin layer of carbon to help with conductivity, as the AAO is an insulating material which charges significantly under exposure to the SEM beam. It does not obstruct our ability to image the surface, as can be seen by the images in Fig S9 and Fig S10. While there is potentially a small amount of Mg and Mn re-deposited on other surfaces of the cross section during the FIB process, the Mg and Mn signals are clearly increased in the region of the magnesiated MnO_2 film. The aluminum signals are visible where AAO is present, while oxygen is concentrated in the regions of MnO_2 and AAO as expected. Since a layer of Pt was sputtered for protection, the signal is pervasive over the whole cross-section, although there is a higher concentration where it was sputtered as a current collector on top of the AAO (Figure S10b). The EDS mapping and line scan give additional proof that Mg is inserting into the bulk of the MnO_2 film.

References

1. C. Julien, M. Massot, R. Baddour-Hadjean, S. Franger, S. Bach and J. P. Pereira-Ramos, *Solid State Ionics*, 2003, **159**, 345-356.
2. M. C. Biesinger, B. P. Payne, A. P. Grosvenor, L. W. M. Lau, A. R. Gerson and R. S. C. Smart, *Applied Surface Science*, 2011, **257**, 2717-2730.